



Published in final edited form as:

Cancer Res. 2021 November 01; 81(21): 5477–5490. doi:10.1158/0008-5472.CAN-20-4028.

Macrophage-derived cholesterol contributes to therapeutic resistance in prostate cancer

Asmaa El-Kenawi^{1,2,3,*}, William Dominguez-Viqueira⁴, Min Liu⁵, Shivanshu Awasthi¹, Julieta Abraham-Miranda¹, Aysenur Keske³, KayLee K. Steiner³, Leenil Noel³, Amparo N. Serna¹, Jasreman Dhillon⁶, Robert J. Gillies², Xiaoqing Yu⁷, John M. Koomen^{5,8}, Kosj Yamoah^{1,9}, Robert A. Gatenby¹⁰, Brian Ruffell^{3,11,*}

¹Department of Cancer Epidemiology, H. Lee Moffitt Cancer Center and Research Institute, Tampa, Florida 33612, USA

²Department of Cancer Physiology, H. Lee Moffitt Cancer Center and Research Institute, Tampa, Florida 33612, USA

³Department of Immunology, H. Lee Moffitt Cancer Center and Research Institute, Tampa, Florida 33612, USA

⁴Small Animal Imaging Lab, H. Lee Moffitt Cancer Center and Research Institute, Tampa, Florida 33612, USA

⁵Proteomics and Metabolomics Core, H. Lee Moffitt Cancer Center and Research Institute, Tampa, Florida 33612, USA

⁶Department of Pathology, H. Lee Moffitt Cancer Center and Research Institute, Tampa, Florida 33612, USA

⁷Department of Biostatistics and Bioinformatics, H. Lee Moffitt Cancer Center and Research Institute, Tampa, Florida 33612, USA

⁸Department of Molecular Oncology, H. Lee Moffitt Cancer Center and Research Institute, Tampa, Florida 33612, USA

⁹Department of Radiation Oncology, H. Lee Moffitt Cancer Center and Research Institute, Tampa, Florida 33612, USA

¹⁰Department of Radiology, H. Lee Moffitt Cancer Center and Research Institute, Tampa, Florida 33612, USA

¹¹Department of Breast Oncology, H. Lee Moffitt Cancer Center and Research Institute, Tampa, Florida 33612, USA

Abstract

*Correspondence: Asmaa.Elkenawi@moffitt.org, (A.E.), **Contact:** Brian Ruffell, Ph.D., H. Lee Moffitt Cancer Center, 12902 Magnolia Drive SRB-2, Tampa, FL, 33612, Voice: 813-745-6305, Brian.Ruffell@moffitt.org (B.R.).

Author Contributions: Conceptualization, A.E., K.Y. and B.R.; Methodology, A.E., J.A.M., A.S., and M.L.; Formal Analysis, A.E., S.A., J.D., X.Y.; Investigation, A.E., W.D.V., M.L., A.K., K.S., L.N., Writing – Original Draft, A.E. and B.R.; Writing – Review & Editing, A.E., K.Y., X.Y., J.K., R.A.G. and B.R.; Visualization, A.E. and B.R.; Supervision, R.G., J.K., K.Y., R.A.G. and B.R.; Funding Acquisition, K.Y. R.A.G. and B.R.

Castration-resistant prostate cancer (CRPC) is a lethal stage of disease in which androgen receptor (AR) signaling is persistent despite androgen deprivation therapy (ADT). Most studies have focused on investigating cell-autonomous alterations in CRPC, while the contributions of the tumor microenvironment are less well understood. Here we sought to determine the role of tumor-associated macrophages in CRPC, based upon their role in cancer progression and therapeutic resistance. In a syngeneic model that reflected the mutational landscape of CRPC, macrophage depletion resulted in a reduced transcriptional signature for steroid and bile acid synthesis, indicating potential perturbation of cholesterol metabolism. As cholesterol is the precursor of the five major types of steroid hormones, we hypothesized that macrophages were regulating androgen biosynthesis within the prostate tumor microenvironment. Macrophage depletion reduced androgen levels within prostate tumors and restricted androgen receptor (AR) nuclear localization *in vitro* and *in vivo*. Macrophages were also cholesterol-rich and were able to transfer cholesterol to tumor cells *in vitro*. AR nuclear translocation was inhibited by activation of Liver X Receptor (LXR)- β , the master regulator of cholesterol homeostasis. Consistent with these data, macrophage depletion extended survival during ADT and the presence of macrophages correlated with therapeutic resistance in patient-derived explants. Taken together, these findings support the therapeutic targeting of macrophages in CRPC.

Keywords

Prostate cancer; macrophages; cholesterol; androgens; androgen receptor; biosynthesis; metabolism

Introduction

Prostate cancer is the second leading of cancer death in men in the United States. Androgen hormones drive prostate cancer cell proliferation and progression by activating the androgen receptor (AR). Given their tumor-promoting role, reducing androgen levels or signaling by using Androgen Deprivation Therapy (ADT) is the standard approach to treat advanced prostate cancer (1,2). Traditionally ADT is achieved by using a gonadotropin-releasing hormone (GnRH) targeting agents (e.g., leuprorelin) which reduce gonadotropin luteinizing hormone (LH) secretion and subsequently decrease systemic androgens (1–3). ADT can also involve androgen synthesis inhibitors (e.g., abiraterone) or AR antagonists that directly inhibit androgen-AR signaling (e.g., bicalutamide or enzalutamide) (3). In most cases ADT induces tumor regression; however, resistance eventually develops and the disease relapses as Castration-Resistant Prostate Cancer (CRPC) (4,5). Androgen-AR signaling persists in many cases of CRPC via alterations in the AR gene, deregulation of AR binding-proteins (2) and/or intratumoral synthesis of androgens (6); thus, both androgen synthesis inhibitors and AR inhibitors can extend survival (7). However, while much is known regarding the intrinsic mechanisms of AR reactivation within tumor cells, little is understood regarding the contributions of the tumor microenvironment in therapeutic resistance in CRPC.

Macrophages are the most abundant immune subpopulation in many solid tumors, wherein they adopt a maladaptive phenotype and are commonly known as tumor-associated macrophages (TAMs) (8). In addition to their role in creating the immunosuppressive

microenvironment in tumors (9), TAMs can promote tumor growth and resistance to therapy through the release of cytokines and angiogenic mediators (10,11). More recently, TAM-secreted metabolites have emerged as a driver of drug resistance. TAM-derived pyrimidines diminished the efficacy of gemcitabine in pancreatic cancer through molecular competition during drug uptake, while in a model of colon cancer, TAMs were involved in the production of glucocorticoids and impaired the efficacy of immune checkpoint blockade (12). Whether macrophage-tumor cell metabolic interactions dictate therapeutic responses in prostate cancer is unknown.

Here we sought to determine the role of macrophages in CRPC using a murine model that recapitulated the high AR signaling and mutational landscape of prostate cancer. We developed orthotopic systems derived from an inducible, autochthonous model of *Trp53/Pten*-deficiency with or without the most common *ETS* rearrangement, *TMPRSS2/ERG* fusion. We then performed transcriptomic and metabolomic characterization of prostate tumors following macrophage depletion. Combined with efficacy studies and *in vitro* experiments, our data demonstrate that macrophages promote AR signaling and castration resistance via enhanced tumor cell cholesterol influx and androgen biosynthesis.

Materials and Methods

Patient-derived explants:

Tumor tissue was obtained from patients undergoing radical prostatectomy at Moffitt Cancer Center. All prostate tissues utilized for this study were collected as part of Moffitt Cancer Center's Total Cancer Care protocol (MCC#14690). Prior to the collection of any prostate tissue all patients provided written informed consent to participate in the MCC#14690 protocol. This study and all collections were conducted in accordance with the U.S. Common Rule and received full Institutional Review Board approval. PDEs were established as previously described (13). Briefly, veterinary dental sponges (Cat. #96002, Novartis) were placed in 24-well plates and soaked in explant media containing IMEM with 5% heat-inactivated FBS, 100 U/mL penicillin/streptomycin, 0.01 mg/ml hydrocortisone (Sigma) and 0.01 mg/ml human recombinant insulin (Life Technologies). Prostate tissue was dissected into 1 mm³ pieces, placed in triplicate on each sponge, conditioned in medium for 48 h then treated at 37°C with or without bicalutamide (10 µM) for additional 4 days. Tissue was harvested after 6 days, formalin-fixed and paraffin embedded (FFPE). For histological analysis, FFPE sections were stained with hematoxylin and eosin (H&E) and CD68 as macrophage marker. Slides were scored by Dr. Jasreman Dhillon and images were analyzed with Aperio eSlide Manager software to estimate nuclei number. Response to bicalutamide is calculated as the ratio between the number of nuclei per mm² in sections obtained from bicalutamide treated PDEs and the number of nuclei per mm² in sections prepared from the corresponding control PDEs. GraphPad PRISM 7 software was used to perform linear regression analysis.

Animal models:

Animals were maintained in the University of South Florida Department of Comparative Medicine barrier facility, and the respective Institutional Animal Care and Use Committee

approved all experiments. The conditional model of prostate cancer was established by crossing $Trp53^{loxP}$ ($Trp53^{tm1Bm/J}$; JAX 008462), $Pten^{loxP}$ ($Pten^{tm1Hwu/J}$; JAX 006440) and C57BL/6-Tg(*Pbsn-cre/Esr1**)14Abch/J mice (JAX 020287), with or without expression of the *TMPRSS2/ERG* fusion gene under control of the Rosa26 promoter and a loxP-flanked stop sequence ($B6.129-Gt(ROSA)26Sor^{tm1(TMPRSS2/ERG)Key/J}$; JAX 024512). The *Pbsn-cre/Esr1** transgene allows inducible Cre-mediated recombination in the mouse prostate following ad libitum dosing of 500 mg/kg tamoxifen-containing chow for 4 weeks (14). Dual *Abca1/Abcg1*-floxed mice ($B6.Cg-Abca1^{tm1Jp} Abcg1^{tm1Tall/J}$; JAX 021067) were crossed with ($B6.129P2-Lyz2^{tm1(cre)Ifo/J}$; JAX 004781). Male C57BL/6J (JAX 000664; 8-12 weeks of age) mice purchased from The Jackson Laboratory were utilized for orthotopic prostate cancer models and bone marrow isolation. For the orthotopic prostate cancer model, mice were prepared for surgical procedure then prostate was injected with 1×10^5 PTE-82 cells suspended in a 1:1 ratio of PBS and Matrigel. Mice were then randomly assigned to experimental groups and treated with 0.6 mg Lupron Depot (AbbVie Inc.) by subcutaneous injection or 20 mg/kg Enzalutamide (Selleck Chemicals) by oral administration. Enzalutamide was prepared as an oral formulation by dissolving in a mixture of DMSO, PEG30, Tween 80 and H₂O. α CSF1 (clone 5A1, BioXCell) was administered intraperitoneally at 1 mg/mouse, followed by 0.5 mg/mouse every 5 days, as described (15).

Magnetic resonance Imaging (MRI):

All MRI experiments were done in a 7T horizontal magnet (Agilent-Technologies) and Bruker electronics (BioSpec AV3HD), using a 35 mm birdcage coil (Doty Scientific). Mice were anesthetized with 2% isoflurane in O₂ during data acquisition. T2-weighted axial images were acquired with a TurboRARE-sequence (TR/TE= 2446/42 ms, FOV = 35×35 mm², image size 256×256 and 21 slices of 1.3 mm thickness and non-fat-suppression). Tumor volume analyses were performed by manual segmentation using in-house written scripts in Matlab (Mathworks Inc.).

Cell lines:

Male-derived murine RAW 264.7 macrophages and the TRAMP-C2 prostate cancer cell line were purchased from ATCC, maintained and cultured according to their suggested protocols. ERG⁻ (PT-83, PT-25, PT-09) and ERG⁺ (PTE-24, PTE-82) syngeneic cell lines (all *Pten*- and *Trp53*-deficient) were generated from tamoxifen treated male mice bearing end-stage prostate tumors as described by others (16). All cell lines lacked expression of CD45 or smooth muscle actin (α -SMA), expressed variable levels of androgen receptor, and expressed detectable keratin 14 and 18. Cells were maintained in Dulbecco modified Eagle's minimal essential medium (DMEM), 25.0 mM glucose, 25.0 mM HEPES supplemented with 10% fetal calf serum (FCS), 2% penicillin/streptomycin, 0.005 mg/ml bovine insulin and 10 nM dehydroisoandrosterone (DHEA). PTE-82 cell line was authenticated for being pathogen free before injection into mice using the Cells, Cell lines, & Biologics Characterization service, University of South Florida, Division of Comparative Medicine. Mycoplasma testing was performed on PTE-82 cells using the Universal Mycoplasma detection kit (ATCC) on December 13, 2020 and were validated to be mycoplasma free. RAW 264.7 macrophages and the TRAMP-C2 prostate cancer cell lines were directly purchased from ATCC, were not tested for mycoplasma, and were used below passage

number 10. Subculturing was performed when cells reached 90% confluency and only passage numbers below 10 (PTE-82) or 14 (PTE-24) were used for *in vivo* or *in vitro* experiments.

Primary cells:

Bone marrow-derived macrophages (BMDMs) were generated as described previously (17,18). In brief, bone marrow was flushed from femurs and tibias of male C57BL/6J mice and cultured at 37°C for 6-7 days in complete macrophage medium (Dulbecco modified Eagle's minimal essential medium (DMEM), 25.0 mM glucose, 25.0 mM HEPES, supplemented with 10% fetal calf serum (FCS), 2% penicillin/streptomycin, and 20 ng/ml M-CSF (R&D Systems).

Flow cytometry:

Mice were cardiac perfused with PBS containing 10 U/ml heparin to clear peripheral blood followed by surgical excision of prostate tissue and/or tumors. Single cell suspensions were then prepared by incubating minced tissue in 1 mg/ml collagenase (Roche) and 50 U/ml DNase I (Roche) at 32°C with agitation for 30 min. The resulting cell suspensions were passed through a 70 µm cell strainer and washed once with FBS-containing DMEM followed by once with PBS. Single cell suspensions were then incubated in ACK Lysing Buffer at RT for 3-5 min. Single cell suspensions were then stained immediately or stored in freezing medium (5% charcoal-stripped serum [CSS], 10% DMSO and 85% DMEM) at -80°C for later analysis. Staining protocol involved incubation with live/dead (L/D) fixable fluorescent reactive dyes (Molecular Probes) in PBS for 10 min. After washing, cells were incubated for 30 min at 4°C in 100 µl staining buffer (PBS, 2% BSA) containing antibodies. For intracellular lipid staining, single cell suspensions were incubated with 0.25 µM Bodipy™ 493/503 in PBS for 15 min at RT. Paraformaldehyde Solution, 4% in PBS (Affymetrix) was used to fix cells. Data was recorded on a LSR II Flow Cytometer (BD Biosciences) and analysis completed using FlowJo software. For the isolation of tumor macrophages, single cell suspensions from *Pten^{pce-/-}Tip5^{pce-/-}* tumors collected under sterile conditions were incubated with a biotinylated anti-mouse F4/80 antibody for 10 min at 4°C, followed by washing with staining buffer, then incubating with streptavidin-coated magnetic beads for 10 min at 4°C. Washed single cell suspensions were placed in a magnetic field and the undesired cells were separated from F4/80⁺ cells by decanting. The last step was repeated 3-4 times to increase purity.

LDL uptake:

Tumor cells were seeded in culture plates and starved for 48 h in 5% CSS DMEM. RAW 264.7 cells were starved for 24 h in 5% CSS DMEM then labeled with pHrodo™ Red-LDL (L34356) 1:2000 for the last 3 h. Tumor cells were then co-cultured with labeled RAW 264.7 cells for another 24 h in serum-free medium. Samples were then processed for flow cytometry by staining with CD45-APC and DAPI. Cells were mixed just prior to acquisition on the LSR II for the 0 min incubation.

Co-culture:

3000 tumor cells were seeded in each well of 96 well plate, then 1000 macrophages were added on the following day in DMEM (phenol red free, contains 25 mM glucose and 25 mM HEPES) supplemented with charcoal stripped serum (CSS) with or without serial dilutions of enzalutamide (10, 20, 40, 80 μ M). Time lapse microscopy measurements were performed every 6-8 h in phase-contrast white light using Incucyte Zoom system (Essen Bioscience). Percent confluency was calculated for each time point using a tailored algorithm for each cell line, and data were normalized to initial time point of each well.

Confocal immunofluorescence:

Cells on chamber slides were washed twice with PBS, fixed with paraformaldehyde solution, 4% in PBS for 20 min and permeabilized with 0.1% Triton X-100 for 5 min. Cells were washed twice with PBS, blocked with 2% BSA in PBS for 1 hr and subsequently incubated with anti-androgen receptor antibody (1:400, Abcam) at 4°C overnight. Cells were washed 3 times with PBS and incubated with appropriate fluorescent-labeled secondary antibodies at RT for 1 hr, followed by incubating with F4/80-APC (1:400) for 1h RT in the case of macrophage co-culture experiments. VECTASHIELD® Antifade containing DAPI was used as mounting medium. Vybrant™ Alexa Fluor™ 555 Lipid Raft Labeling Kit was utilized according to the manufacturer's instructions. Images were visualized using Leica TCS SP8 laser scanning microscope (Leica Microsystems) and Images were exported in TIF format with LAS X software version 3.1.5 (Leica Microsystems). Mean fluorescence intensity (MFI) analysis was performed on the TIF images with Definiens Tissue Studio version 4.7 (Definiens AG). In the software the nucleus detection (DAPI channel) and cell shape (combination of Green and Red channel) algorithms were used to segment individual cells (including nucleus and cytoplasm identification) within each image. Using this cell segmentation, the MFI for nucleus, cytoplasm, and cell compartments were calculated for each image. The nucleus to cytoplasm AR intensity ratio was plotted using the basic (generic) R command hist using R studio version 4.0.3. A smooth curve was fitted to the histogram using kernel density estimation computed by the density function. We then computed the percent of AR^{hi} cells per each image by setting the threshold to the 3rd quartile of the cancer cell + macrophage condition.

Histology and immunohistochemistry (IHC):

Histological specimens were embedded in paraffin, sectioned (4 μ m slices) and left unstained or stained with haematoxylin & eosin (H&E). For immunohistochemistry, slides were stained using a Ventana Discovery XT automated system (Ventana Medical Systems). Briefly, slides were deparaffinized on the automated system with EZ Prep solution (Ventana). Enzymatic retrieval method was used in Protease 1 (Ventana). The rabbit primary antibodies that react to AR (1:200, Abcam), F4/80 (1:100, Abcam), α -SMA (1:250, Abcam), Ly6G (1:100, Biolegend), CD3 (1:200, Abcam), Ki67 (1:300, Abcam), in Dako antibody diluent (Agilent) and incubated for 60 min. The Ventana OmniMap Anti-Rabbit Secondary Antibody was used for 8 min. The detection system used was the Ventana ChromoMap kit, and slides were then counterstained with hematoxylin, followed by dehydration and cover-slipping. Histology slides were scanned using the Aperio™

ScanScope XT with a 200X-(0.8NA) objective lens at a rate of 5 minutes per slide via Basler tri-linear-array. Images were analyzed with Aperio eSlide Manager software using nuclear (AR), membrane (F4/80), or pixel (SMA, Ly6G, Ki67) detection algorithms. The positive staining categories (weak, moderate, strong) on the default nuclear detection algorithm were tailored to account for the tumor AR staining, and the % of cells with strong staining is shown as AR^{hi}. All Intensity thresholds remained consistent for each image within the respective biomarker group.

LC-MS/MS:

Liquid Chromatography-Mass Spectrometry (LC-MS) was performed using a UHPLC (Vanquish, Thermo Scientific) interfaced with a Q Exactive HF hybrid quadrupole-Orbitrap mass spectrometer (Thermo Scientific, San Jose, CA). Chromatographic separation was conducted on an Accucore C18 column (2.1 mm ID x 100 mm in length with 2.6 μ m particle size) maintained at 40°C. Separation was achieved using mobile phases A (100% H₂O with 0.1% formic acid) and B (100% MeOH with 0.1% formic acid). The gradient was programmed as follows: 2 minutes at 30% B, then ramping from 30% B to 90% B over 12 minutes, washing with 90% B for 2 minutes, returning to 30% B over 0.1 minutes and re-equilibrating for 3.9 minutes for a total run time of 20 minutes. The flow rate was set to 0.250 mL/min except 16.1-19 min, where the flow rate was increased to 0.450 mL/min for re-equilibration. For MS, parallel reaction monitoring (PRM) was used for the detection and quantification. The instrument settings were as follows: sheath gas 50, auxiliary gas 10, sweep gas 1, spray voltage 3.5 kV, capillary temperature 325°C, S-lens RF level 50, auxiliary gas temperature 350°C, resolution 30,000, AGC target 2E5, and isolation window width 1.5 m/z with an offset of 0.4 m/z. The data analysis is performed using XCalibur. A processing method was created based on the precursors and fragments listed in Fig. S2. The m/z and RT tolerance values were 5 ppm and 0.05 min. The sum of the peak heights of all the fragments for each analyte is used for quantification. To calculate the amounts of androgen in the sample, the ion signal for the endogenous androgen was divided by the ion signal for the corresponding SIS and multiplied by the amount of SIS (in pg) spiked into each sample that was injected on column. To enable more effective comparison between samples, final results are normalized by tissue weight and expressed as pg androgen/mg tissue.

Real-time quantitative PCR:

RNA was extracted using RNeasy isolation kit (Qiagen). Real-time quantitative PCR (RT-qPCR) was then carried out using TaqMan™ RNA-to-CT™ 1-Step Kit (Thermo Fisher Scientific). PCR was performed using individual TaqMan Assays with catalogue numbers provided in Supplementary Table 1 with searchable Research Resource Identifier (RRID). Relative Expression/Fold Change was calculated by using 2^{-Ct} method where Ct = Average Ct Gene of Interest - Average Ct of *Tbp* as Endogenous Control.

TCGA PRAD analysis:

The correlation of macrophage-related genes and de novo cholesterol biosynthesis in a prostate cancer cohorts was computed using level 3 gene expression estimates from the

RNA-Sequencing in the TCGA PRAD (Prostate Adenocarcinoma Data Set) database, extracted, and hosted by cBioPortal for Cancer Genomics (www.cbioportal.org).

GRID registry:

To evaluate the clinical relevance of macrophages in therapeutic resistance to ADT we utilized 635 prostatectomy tumor samples with whole transcriptome data from the Decipher GRID™ registry data (NCT02609269, institutional review board approved) (19). Gene expression markers of tumor macrophages were used to evaluate their correlation with the ADT response score, a validated gene expression signature used in the prediction of postoperative ADT response, as has been described(20).

Statistical Analysis:

Unless otherwise indicated, unpaired t test was used to facilitate comparisons between two group means. For multiple group comparisons two-way ANOVA was used. Data points represent biological or technical replicates and are shown as the mean ± SEM or SD as indicated in the figure legends. Intergene correlation matrix with hierarchical clustering, based on spearman correlation coefficient, was used determine correlation clusters. All statistical tests were two sided and are shown as *p<0.05, **p <0.01, ***p<0.001 (described in each figure legend). Statistical analysis was carried out using R studio v3.5.0 and GraphPad PRISM 7 software.

Results

Development of syngeneic mouse models of prostate cancer

Prostate cancers often harbor recurrent rearrangements of the E26 Transformation-Specific (ETS) family of transcription factors. Among these, fusion of ETS-related gene (*ERG*) to the membrane protease *TMPRSS2* (*TMPRSS2-ERG*) represents the most common structural rearrangement in prostate cancer (21). We established a mouse model that reflects the mutational landscape of aggressive prostate cancer by crossing *Trp53^{lox}*, *Pten^{loxP}* and *Pbsn-cre/Esr1** mice, with or without the *TMPRSS2/ERG* fusion gene (Fig. 1A). Cre-mediated recombination was confirmed in the mouse prostate 2 months following the initiation of tamoxifen, as shown by immunohistochemistry staining of GFP and increased Ki67 positivity (Fig. 1B). Both *Pten^{pce-/-} Trp53^{pce-/-}* and *Pten^{pce-/-} Trp53^{pce-/-} TMPRSS2-ERG^{pce+}* mice began to develop tumors after 6 months, as detected by MRI, with all mice developing tumors within 12 months (Fig. 1C). In line with the putative oncogenic role of ETS fusions in prostate cancer (22), there was an increase in tumor incidence and progression, and reduced survival in *TMPRSS2-ERG^{pce+}* mice (Fig. 1C). Neoplastic progression at 6 and 12 months (Fig. 1D) was marked by higher Ki67 positivity and reduced presence of SMA⁺ fibromuscular stroma in both genotypes (Fig. S1A–B). We did not observe metastatic lesions in the liver or lungs of the mice examined. Early tumor lesions were androgen driven as mice (4-month post tamoxifen) treated with Lupron, a gonadotropin-releasing hormone analogue that reduces systemic testosterone levels, displayed decreased tumor lesion size in both genotypes, as shown by representative MRI T2-weighted images (Fig. 1E, S1C–D). From end stage mice we generated a series of syngeneic *TMPRSS2-ERG⁺* (denoted as PTE) and *TMPRSS2-ERG⁻* (denoted as PT)

prostate cancer cell lines that expressed varying levels of cytokeratin 8, 14, and 18 (Fig. 1F) as well as AR (Fig. 1G). As expected, *Pten*-deficiency resulted in sensitivity to the PI3K inhibitor GDC-941 (Fig. S1E). AR nuclear translocation was observed following the addition of dihydrotestosterone (DHT) in all cell lines tested (Fig. 1H). However, cell lines displayed differential sensitivity to enzalutamide, including 3 lines (PTE-82, PT-09, PT-25) that survived even in the presence of 80 μ M enzalutamide, thereby representing models of CRPC (Fig. 1I).

Macrophages are associated with cholesterol transport and androgen synthesis

Both the PT-09 and PTE-82 CRPC cell lines established orthotopic tumors following injection into the prostate glands of C57BL/6J mice. Critically, F4/80⁺ macrophages formed the dominant immune subset in these orthotopic tumors, with Ly6G⁺ neutrophils comprising only a small percentage of the total CD45⁺ population (Fig. 2A). This recapitulated our findings in autochthonous *TMPRSS2-ERG*^{pce+} and *TMPRSS2-ERG*^{pce-} prostate tumors at both 6 and 12 months (Fig. S1A–S1B). In solid tumors the majority of TAMs differentiate from peripheral blood monocytes under the influence of colony stimulating factor-1 (CSF-1), with a smaller population of tissue-resident macrophages that persist through *in situ* proliferation (23–25). To determine the role of macrophages in CRPC, we treated mice bearing orthotopic PTE-82 tumors with an α CSF-1 neutralizing antibody for 7 days (Fig. 2B), which reduced the percentage of CD11b⁺F480⁺ TAMs without altering the frequency of other immune subsets (Fig. S2A). Another group of mice were treated with 0.6 mg/mouse Lupron Depot 16 days prior to tumor collection and processing for RNA sequencing to provide a comparison to standard-of-care therapeutics.

As shown in Fig. 2C, RNA sequencing followed by gene set enrichment analysis (GSEA) revealed that α CSF-1 treatment decreased the expression of genes related to steroid metabolism, bile acid metabolism and adipogenesis. Interestingly, these changes were very similar to those observed following treatment with Lupron (Fig. 2C, S2B). Depletion of TAMs elicited decreased expression of many AR-regulated genes (e.g. endogenous *Tmprss2*), along with a decrease in the global AR signature (normalized ES –1.3508) nearly equivalent to Lupron (normalized ES –1.4494) (Fig. 2D–S2C). As cholesterol is the main precursor of bile acids and the five major types of steroid hormones, the results suggested that depletion of TAMs was causing a perturbation in cholesterol transport and/or metabolism. We reasoned that this perturbation could interfere with androgen biosynthesis in the tumor microenvironment, thereby explaining the reduced AR signature observed following TAM depletion. To evaluate this possibility, we utilized a LC-MS/MS metabolomics platform to quantify the level of intra-tumoral androgens in mouse tissues (Fig. S2D) (26). Treatment with α CSF-1 significantly decreased the amount of the most potent endogenous androgen and final product, DHT (Fig. 2E, S2E). No significant changes in the upstream steroids were observed. Combined, these data indicate that macrophages regulate androgen biosynthesis in CRPC, potentially through a role in cholesterol transport/metabolism.

Macrophages directly regulate AR nuclear translocation and resistance to enzalutamide

The AR functions by binding steroid hormones in the cytoplasm and translocating to the nucleus, where, in conjugation with co-factors, it regulates expression of target genes by binding to specific DNA sequences known as androgen response elements (27). Based upon the reduction in intratumoral DHT and the AR gene signature that followed depletion of TAMs (Fig. 2D–E), we measured the amount of AR nuclear localization within tumors following administration of α CSF-1. Nuclear AR staining was prevalent in control tumors (Fig. 3A) and correlated with infiltration by F4/80⁺ macrophages (Fig. S3A). In contrast, the reduction in TAMs that followed administration of α CSF-1 coincided with a significant reduction in nuclear AR (Fig. 3A–B). This was not due to reduced AR protein expression in α CSF-1 treated tumors, but rather sequestration of AR in the cytosol. Notably, the reduction in AR nuclear translocation following TAM depletion was equivalent to treating mice with Lupron (Fig. 3A). In addition, upon analyzing autochthonous *TMPRSS2-ERG*^{pce+} at 6 and 12 months, we found a positive correlation between nuclear localization of AR and the extent of macrophage infiltration (Fig. S3B). Nuclear localization of AR did not correlate with the presence of stroma in general, as there was no association with α -SMA ($R^2 = 0.003$). Intriguingly, this correlation was not observed in autochthonous *TMPRSS2-ERG*^{pce-} tumors (Fig. S3B). Thus, TAMs regulate AR activation and nuclear translocation, at least in CRPC tumors expressing an ETS fusion gene.

We next sought to determine whether macrophages could directly induce AR nuclear translocation. We first established an *in vitro* system incubating tumor cells under androgen-deprived conditions (i.e., 5% CSS). We then evaluated the ability of bone marrow-derived macrophages (BMDMs) to promote AR nuclear localization by quantifying the ratio of nuclear to cytoplasmic AR on a cell-by-cell basis and percent of cells with high AR nuclear expression (Fig. 3C). As shown in Fig. 3D–E, the addition of BMDMs induced a significant increase in AR nuclear localization in the 3 different cell lines examined, evident by both histogram and the percentage of cells with high AR nuclear expression. These results were recapitulated using F4/80⁺ TAMs isolated from orthotopic tumors (Fig. S3C–E). In contrast, we found no increase in AR nuclear localization when tumor cells were incubated with conditioned medium from IL-4-stimulated BMDMs (Fig. S3F).

F4/80⁺ TAMs also induced the expansion of GFP⁺ PTE-24 cells in androgen-deprived conditions (Fig. S3G). Similarly, BMDMs promoted the proliferation of PTE-24 and PTE-82 cells, as well as protected against the cytotoxicity of the AR inhibitor enzalutamide (Fig. 3F, S3H). However, consistent with the high level of enzalutamide resistance observed in the PTE-82 cell line (Fig. 1I), the relative impact of BMDMs was reduced. Interestingly, the effect of DHT on proliferation by these cell lines positively correlated with the growth induced by the presence of BMDMs (Fig. S3I). Combined, these data demonstrate that tumor macrophages can directly promote AR nuclear localization and resistance to AR inhibitors.

Macrophages regulate cholesterol bioavailability

We were intrigued by our comparative transcriptomic studies showing downregulation of bile acid- and steroid biosynthesis-related genes in tumors isolated from α CSF1 treated

mice, which suggested altered cholesterol metabolism. We thus performed correlation analysis between macrophage-related genes (*CSF1R*, *CD68*, *CD206*, *CD163*) and genes involved in bile acid and lipid metabolism in TCGA data (Prostate Adenocarcinoma dataset, Cell 2015) (28). We observed that macrophage-related genes correlated with those related to cholesterol transport, such as *ABCA1*, *ABCA8*, *ABCA6* (Fig. 4A). Since cellular cholesterol is maintained by a balance between uptake and synthesis, we queried whether *de novo* cholesterol synthesis might be reduced in the presence of high macrophage infiltrate, and observed an inverse correlation between macrophage markers and *de novo* cholesterol synthesis-related genes (*ACAT2*, *HMGCR*, *HMGCS1*, *SQLE*) in two prostate cancer patient datasets (Fig. 4B, S4A). *HMGCR* and *SQLE* encode enzymes that regulate rate limiting steps in the *de novo* cholesterol synthesis pathway essential for prostate cancer cell survival (Fig. S4B), and inhibiting the mevalonate pathway rate-limiting enzyme HMGCR (using atorvastatin), farnesyl diphosphate synthase (using zoledronate) or fatty acid synthesis (using cerulenin) all resulted in cell death in the murine prostate cancer cell lines (Fig. S4C).

Cholesterol is mostly stored in the form of cholesteryl esters in intracellular lipid droplets. Accordingly, we quantified the lipid content of immune cells within tumors and found that TAMs had the highest level of lipid content, both in orthotopic and autochthonous *TMPRSS2-ERG^{pcc+}* tumors (Fig. 4C, S4D–E). BMDMs also expressed numerous genes related to cholesterol influx/efflux at higher levels than the prostate cancer cell lines, including *Abca1*, *Abcg1*, *Cd36*, *Lpl* and *Scarb1* (Fig. 4D). To evaluate if macrophages were capable of transferring cholesterol to tumor cells, we loaded RAW264.7 cells, a murine macrophage cell line, with pHrodo-Red conjugated LDL as a source of cholesterol (and associated fatty acids and proteins). Note that pHrodo is fluorescent only at an acidic pH, signifying intracellular uptake via endocytosis and/or phagocytosis has occurred (Fig. 4E). Pre-loaded RAW264.7 cells were then co-cultured with the prostate cancer cell lines for 24 hours, and depending on the tumor cell line, up to 40% of the cancer cells acquired derived components of LDL (Fig. 4E).

To evaluate whether prostate cancer cells were promoting cholesterol outflow by macrophages, we labeled cells with cholera toxin subunit B (CTB; a surrogate marker for membrane cholesterol). As shown in Fig. 4F, co-culture with cancer cells largely eliminated CTB labeling of RAW264.7 cells, demonstrating a reduction in plasma membrane cholesterol. Finally, we sought to determine if the presence of macrophages could promote the acquisition of cholesterol (or other LDL components) by adding pHrodo-Red conjugated LDL to prostate cancer cells and RAW264.7 cells (Fig. 4G). RAW264.7 cells rapidly took up LDL and were mostly positive during the first image acquisition, but fluorescent signal began to appear in the adherent prostate cancer cells within 2 hours. In contrast, no fluorescent signal was observed when prostate cancer cells were incubated alone (Fig. 4G). Overall, these data suggest that macrophages are a rich source of cholesterol and are capable of transferring cholesterol to prostate tumor cells.

Activating LXR β inhibits macrophage-mediated AR translocation in tumor cells.

Our cancer cell lines expressed detectable, albeit low, levels of the first two enzymes required for the conversion of cholesterol into androgens (*Cyp11a*, *Cyp17a*), whereas

we were unable to detect gene expression of the enzyme responsible for cholesterol side-chain cleavage (*Cyp11a*) in BMDMs (Fig. S5A). We therefore sought to determine if preventing cholesterol transfer between macrophages and tumor cells could restrict AR nuclear translocation as a surrogate of androgen production. MetaCore analysis of our RNAseq data revealed that tumors with high macrophage infiltration (i.e. IgG control) were enriched in a Liver X Receptor (LXR)-regulated transcriptional program including target genes such as *Abca1*, *Abcg1*, *Scarb1* and *Cd36*. Macrophages are generally thought to unload cholesterol via efflux mediated via the ATP-binding cassette transporters A1 and G1 (ABCA1 and ABCG1) to apolipoprotein A1 and high-density lipoproteins (HDLs), respectively, a process known to regulate atherosclerosis (29–31). Macrophage expression of these transporters has also recently been shown to promote the growth of ovarian cancer (32). We therefore crossed *Abca1^{fl/fl}/Abcg1^{fl/fl}* mice with *LysM-Cre⁺* mice to generate myeloid-specific loss of ABCA1 and ABCG1. Surprisingly, the extent of AR nuclear positivity within orthotopic tumors was equivalent in *LysM-Cre⁻* and *LysM-Cre⁺* animals (Fig. 5A). There was also no difference in the growth of orthotopic tumors between the two genotypes (Fig. 5B). Consistent with this, BMDMs generated from *LysM-Cre⁻* and *LysM-Cre⁺* mice were equally capable of inducing AR nuclear translocation (Fig. 5C). AR nuclear translocation *in vitro* was similarly unchanged by a blocking antibody against CD36 or the addition of a specific scavenger receptor class B type I (SR-B1, encoded by *Scarb1*) inhibitor, BLT-1 (Fig. S5B).

It has recently been shown that macrophages have the ability to transfer cholesterol through direct transcellular cholesterol movement in an ABCA1/G1-independent manner (33). Although the molecules involved in this process are unknown, upon re-examining our live imaging data we noticed that pHrodo-Red fluorescence in cancer cells occurred within those in proximity to RAW264.7 cells (Fig. 4E). We therefore sought to determine if inhibiting cholesterol influx and/or inducing cholesterol efflux in tumor cells would restrict AR nuclear translocation by activating the LXR transcription factors, which function as the master regulators of cholesterol homeostasis. Both BMDMs and prostate cancer cells expressed detectable levels of the genes encoding LXR α (*Nr1h3*) and LXR β (*Nr1h2*); however, *Nr1h2* was expressed at much higher levels than *Nr1h3* in the prostate cancer cell lines (Fig. 5D). As expected, the LXR α β inverse agonist, SR943, downregulated expression of *Abca1* in cancer cells, while an LXR β agonist currently in clinical trials, RGX-104, had the reverse effect (Fig. S5C). RGX-104 was also able to functionally inhibit prostate cancer cells from taking up pHrodo-Red LDL during a 24-hour incubation (Fig. S5D). We therefore examined the ability of SR943 and RGX-104 to inhibit AR nuclear translocation during BMDM and prostate cancer cell co-culture. As shown in Fig. 5E, SR943 only slightly reduced the extent of AR in the nucleus, while RGX-104 completely prevented AR nuclear translocation induced by the presence of BMDMs. This was not due to a direct effect on basal AR activity as expression of the AR target gene, *Fkbp5*, was not impacted by either the inverse agonist or agonist when BMDMs were not present (Fig. S5E). Collectively, these data demonstrate that cholesterol exchange between macrophages and prostate tumor cells enhances AR activation.

Macrophage depletion sensitizes prostate cancer to ADT

Based upon the ability of TAMs to regulate the level of intratumoral androgens (Fig. 2E), AR nuclear localization (Fig. 3A) and AR-dependent gene expression (Fig. 2D), we sought to assess whether macrophage infiltration was associated with resistance to ADT using an *ex vivo* patient-derived explant (PDE) system. PDEs are established by culturing patient tissues immediately after surgical removal of the prostate (Fig. 6A) and maintain hormonal response, cellular interactions and a patient-specific tumor microenvironment (13). We treated tumor tissues explants from 5 patients (34) with the AR targeting agent bicalutamide for 4 days and quantified the number of nuclei between control and treated conditions to measure response to bicalutamide, as well as macrophage infiltration by CD68 immunohistochemistry. As shown in Fig. 6B and 6C, resistance to bicalutamide positively correlated with infiltration by CD68⁺ macrophages, suggesting a role of macrophage in limiting response to ADT. We next sought to evaluate the relevance of these findings within the Decipher GRIDTM registry data of 635 prostatectomy tumor samples with whole transcriptome data. As macrophages and AR nuclear localization were only correlated in the *TMPRSS2-ERG*^{cc+} murine model (Fig. S3B) we stratified patients by ETS status and compared the ADT response signature with expression of macrophage-associated genes (*CD68*, *CD163*, *CSF1R*, or *MRC1*). In ETS⁺ tumors we found that the genomic ADT response signature was inversely correlated with the presence of macrophages, whereas this association was not observed in ETS⁻ tumors (Fig. 6D).

Based upon the relationship between macrophage infiltration and the genomic response signature in ETS⁺ tumors we next sought to evaluate if depleting TAMs could reduce tumor growth and/or enhance survival in the *TMPRSS2-ERG*⁺ orthotopic CRPC model system. Orthotopic PTE-82 tumors were insensitive to enzalutamide (Fig. S6A), consistent with their resistance to the drug *in vitro*. Subcutaneous TRAMP-C2 were also resistant to enzalutamide (Fig. S6B). We thus evaluated the effect of Lupron *in vivo*, and found a significant reduction in the growth of orthotopic PTE-82 tumors during the early stage of treatment (Fig. S6C–D). Critically, while α CSF1 alone had no impact on tumor growth, the combination of α CSF1 and Lupron resulted in a more significant reduction in tumor volume (Fig. 6E–F). We therefore extended these studies to evaluate survival as measured by tumor size (<1200 mm³), organ obstruction, or overall animal health. Over the course of three independent experiments we observed a significant improvement in survival in PTE-82-tumor bearing mice treated with α CSF1 and Lupron, but not in mice treated with either agent alone (Fig. 6G) Reduced tumor growth did not appear to be driven by changes in T cell infiltration (Fig. S6E), vascular density (Fig. S6F), or other immune populations (Fig. S6G).

Discussion

AR signaling remains active in CRPC and plays a critical role in disease progression (7). Compensatory growth factors secreted by other cell types in the tumor microenvironment are also thought to promote castration resistance (35). Castrating tumor-bearing mice elicits an influx of leukocytes, including B cells, neutrophils, and macrophages into prostate tumors, which are able to drive the emergence of CRPC by regulating senescence and proliferation (36–40). These studies point towards a feed-forward signaling loop in which

cell stress induces expression of chemokines that promote leukocyte accumulation and drive the growth and development of CRPC. Accordingly, reducing infiltration of macrophage and neutrophils through the use of a CSF1R or CXCR2 antagonist, respectively, enhances the efficacy of ADT (37,39). Critically, increased macrophage infiltration has been described in radical prostatectomy samples from ADT-treated patients, and high macrophage infiltration is associated with increased risk of biochemical recurrence (41).

Despite the association between macrophages and CRPC, the mechanism by which TAMs regulate response to ADT is unclear. CD11b⁺Ly6G⁺ myeloid cells in prostate tumors can act as an important source of IL-1 receptor antagonist and IL-23 (39,41), whereas no specific macrophage-derived factors have been shown to drive the development of CRPC. Here we describe how macrophages regulate local steroid biosynthesis via enhancing the uptake of extrinsic cholesterol by prostate cancer cells, thereby leading to AR signaling and resistance to Lupron in a model of CRPC. *De novo* steroidogenesis begins with cholesterol translocation into the mitochondria where the rate-limiting enzyme CYP11A1 converts cholesterol to pregnenolone, followed by series of enzymatic reactions to produce various steroids such as androgens, estrogens or glucocorticoids (42). Recently, glucocorticoids produced by TAMs were shown to elicit T cell dysfunction and resistance to immunotherapy in the MC38 colon carcinoma model (12). However, another recent study reported high expression of *Cyp11a1* by T cells and granulocytes, but not TAMs, within B16-F10 melanoma tumors (43). In our study, we did not detect *Cyp11a1* in BMDMs, pointing towards the transfer of cholesterol rather than pregnenolone or other downstream derivatives *in vitro*. Prostate cancer cells also express most steroidogenic enzymes and have the ability to convert cholesterol to androgens (44–46). However it remains possible that there are other mechanisms by which macrophages regulate steroidogenesis, as reported in early studies investigating modulation of Leydig cell steroidogenesis by testicular macrophages (47).

Lipid transporters and scavenger receptors have emerged as potential targets in various types of solid malignancies (48,49). In the ID8 ovarian cancer model, genetic ablation of *Abca1/Abcg1* in myeloid cells decreased tumor growth, although whether this was through altered macrophage function or reduced cholesterol transfer to tumor cells is unclear (32). Similar to this study, we saw that the presence of tumor cells induced cholesterol efflux in macrophages. However, using the same genetic system we did not observe changes in prostate tumor growth or the ability of macrophages to promote AR nuclear localization *in vitro* or *in vivo*. Indeed, we found that macrophages can directly transfer cholesterol in serum free medium lacking lipoproteins, which would limit the ability of ABCA1/G1 to transfer cholesterol onto HDL particles. Inhibition of the HDL receptor SR-B1 also had minimal impact on the ability of BMDMs to promote AR nuclear localization *in vitro*. Our results are therefore in line with a recent a study that reported transcellular transfer of macrophage cholesterol to smooth muscle cells in the absence of serum or HDL (50). Exchange of cholesterol can occur through exchange of plasma membrane microdomains, release of cholesterol rich-vesicles or through tunneling nanotubes (51–53). Additional work is required to delineate the molecular mechanism by which this transfer occurs within tumors.

In addition to *PTEN* and *TP53* alterations, approximately 40% of prostate cancers carry recurrent rearrangements of the ETS family of transcription factors, of which fusion of *ERG* to the membrane protease *TMPRSS2* represents the most common (54). Murine studies have shown that the *TMPRSS2-ERG* fusion increases early onset invasive prostate cancer through changes in the AR cistrome and enhancing AR output (22). *TMPRSS2-ERG* gene fusion status is also associated with a high androgen-regulated gene expression in early onset prostate cancer (55,56). Apart of the transcriptional impact, *TMPRSS2-ERG*⁺ patients have androgen profiles that differ substantially from *TMPRSS2-ERG*⁻ patients, including increased DHT/testosterone ratios (57). These data are consistent with our preclinical observations regarding the correlation between macrophages and AR nuclear translocation in the autochthonous and orthotopic *TMPRSS2-ERG*⁺ murine model, and with the inverse correlation between macrophage infiltration and the genomic ADT response signature in ETS⁺ patients. Cumulatively, these results suggest that macrophage-targeted agents such as CSF1R inhibitors should be directed towards patients with ETS⁺ prostate cancer.

Collectively, our data show that macrophages deliver cholesterol to prostate tumor cells as an example of metabolic cooperation, thereby increasing intratumoral androgen production and activation of the AR. Whether targeting macrophages, cholesterol transfer, or cholesterol metabolism will prove therapeutically viable in prostate cancer remains to be determined. Interestingly, LXR β agonists induce apoptosis of immunosuppressive myeloid cells through enhanced expression of ApoE, thereby driving T cell responses in melanoma (58–60). Loss of LXR also causes cholesterol accumulation and chronic inflammation in the mouse prostate during castration-induced hypotrophy (61). Combined with their ability to restrict the cholesterol pool required for tumoral androgen synthesis (46), LXR β agonists could therefore have profound impacts on the tumor microenvironment and offer unique opportunities for combinatorial therapies. Regardless of the approach taken, it is likely that macrophage-targeted therapies will display limited efficacy as single agents and that combinatorial approaches utilizing ADT should be evaluated clinically.

Supplementary Material

Refer to Web version on PubMed Central for supplementary material.

Acknowledgements:

The authors would like to thank Noel Clark, Sean Yoder, Antonio Ortiz, Jayden Cline and Joseph Johnson for technical assistance. The authors also thank John Cleveland, Conor Lynch, Jingsong Zhang and Paulo Rodriguez for scientific discussion.

Financial Support:

K.Y. is supported by George Edgecomb Society and Department of Defense award (W81XWH-19-1-0435-PC 18103). R.A.G is supported by the NIH/NCI (U54CA193489) and the V Foundation. B.R. is supported by the NIH/NCI (R00CA185325, R01CA230610), a 2021 Miles for Moffitt Award, and additional internal funding from Moffitt Cancer Center. This work was supported by Moffitt Cancer Center Proteomics and Metabolomics, Small Animal Imaging Lab, Flow Cytometry, Molecular Genomics, Analytic Microscopy, and Tissue Core Facilities, all comprehensive cancer center facilities designated by the National Cancer Institute (P30-CA076292).

Conflict of Interests:

A.E., J.K. and B.R. have courtesy faculty appointments at the University of South Florida, Tampa, FL 33620. A.E. has a faculty appointment at Mansoura University, Mansoura Egypt, 35516. B.R. has received payments from Merck & Co., Inc. and Roche Farma S.A. for consulting, and has had sponsored research agreements with TESARO: A GSK Company unrelated to this study. The other authors declare no potential conflicts of interest.

References

1. Attar RM, Takimoto CH, Gottardis MM. Castration-Resistant Prostate Cancer: Locking Up the Molecular Escape Routes. *Clinical Cancer Research* 2009;15:3251–5 [PubMed: 19447877]
2. Karantanos T, Corn PG, Thompson TC. Prostate cancer progression after androgen deprivation therapy: mechanisms of castrate resistance and novel therapeutic approaches. *Oncogene* 2013;32:5501–11 [PubMed: 23752182]
3. Pu Y, Xu M, Liang Y, Yang K, Guo Y, Yang X, et al. Androgen receptor antagonists compromise T cell response against prostate cancer leading to early tumor relapse. *Science Translational Medicine* 2016;8:333ra47–ra47
4. Nussbaum N, George DJ, Abernethy AP, Dolan CM, Oestreicher N, Flanders S, et al. Patient experience in the treatment of metastatic castration-resistant prostate cancer: state of the science. *Prostate Cancer Prostatic Dis* 2016;19:111–21 [PubMed: 26832363]
5. Sharifi N Minireview: Androgen metabolism in castration-resistant prostate cancer. *Mol Endocrinol* 2013;27:708–14 [PubMed: 23592429]
6. Sharifi N, McPhaul MJ, Auchus RJ. “Getting from here to there”--mechanisms and limitations to the activation of the androgen receptor in castration-resistant prostate cancer. *Journal of investigative medicine : the official publication of the American Federation for Clinical Research* 2010;58:938–44 [PubMed: 21030877]
7. Litwin MS, Tan HJ. The Diagnosis and Treatment of Prostate Cancer: A Review. *JAMA* 2017;317:2532–42 [PubMed: 28655021]
8. El-Kenawi A, Gatenbee C, Robertson-Tessi M, Bravo R, Dhillon J, Balagurunathan Y, et al. Acidity promotes tumour progression by altering macrophage phenotype in prostate cancer. *British journal of cancer* 2019;121:556–66 [PubMed: 31417189]
9. DeNardo DG, Ruffell B. Macrophages as regulators of tumour immunity and immunotherapy. *Nat Rev Immunol* 2019;19:369–82 [PubMed: 30718830]
10. Ruffell B, Coussens LM. Macrophages and Therapeutic Resistance in Cancer. *Cancer cell* 2015;27:462–72 [PubMed: 25858805]
11. El-Kenawi AE, El-Remessy AB. Angiogenesis inhibitors in cancer therapy: mechanistic perspective on classification and treatment rationales. *Br J Pharmacol* 2013;170:712–29 [PubMed: 23962094]
12. Acharya N, Madi A, Zhang H, Klapholz M, Escobar G, Dulberg S, et al. Endogenous Glucocorticoid Signaling Regulates CD8(+) T Cell Differentiation and Development of Dysfunction in the Tumor Microenvironment. *Immunity* 2020;53:658–71 e6 [PubMed: 32937153]
13. Shafi AA, Schiewer MJ, de Leeuw R, Dylgjeri E, McCue PA, Shah N, et al. Patient-derived Models Reveal Impact of the Tumor Microenvironment on Therapeutic Response. *European Urology Oncology* 2018;1:325–37 [PubMed: 30467556]
14. Birbach A, Casanova E, Schmid JA. A Probasin-MerCreMer BAC allows inducible recombination in the mouse prostate. *Genesis* 2009;47:757–64 [PubMed: 19830822]
15. Ruffell B, Chang-Strachan D, Chan V, Rosenbusch A, Ho CM, Pryer N, et al. Macrophage IL-10 blocks CD8+ T cell-dependent responses to chemotherapy by suppressing IL-12 expression in intratumoral dendritic cells. *Cancer cell* 2014;26:623–37 [PubMed: 25446896]
16. Foster BA, Gingrich JR, Kwon ED, Madias C, Greenberg NM. Characterization of prostatic epithelial cell lines derived from transgenic adenocarcinoma of the mouse prostate (TRAMP) model. *Cancer Res* 1997;57:3325–30 [PubMed: 9269988]
17. Zhang X, Goncalves R, Mosser DM. The isolation and characterization of murine macrophages. *Curr Protoc Immunol* 2008;Chapter 14:Unit 14 1

18. Vereyken EJ, Heijnen PD, Baron W, de Vries EH, Dijkstra CD, Teunissen CE. Classically and alternatively activated bone marrow derived macrophages differ in cytoskeletal functions and migration towards specific CNS cell types. *J Neuroinflammation* 2011;8:58 [PubMed: 21615896]
19. Awasthi S, Berglund AE, Abraham-Miranda J, Rounbehler RJ, Kensler KH, Serna AN, et al. Comparative genomics reveals distinct immune-oncologic pathways in African American men with prostate cancer. *Clin Cancer Res* 2020
20. Karnes RJ, Sharma V, Choerung V, Ashab HA, Erho N, Alshalalfa M, et al. Development and Validation of a Prostate Cancer Genomic Signature that Predicts Early ADT Treatment Response Following Radical Prostatectomy. *Clin Cancer Res* 2018;24:3908–16 [PubMed: 29760221]
21. Ahearn TU, Pettersson A, Ebot EM, Gerke T, Graff RE, Morais CL, et al. A Prospective Investigation of PTEN Loss and ERG Expression in Lethal Prostate Cancer. *J Natl Cancer Inst* 2016;108
22. Chen Y, Chi P, Rockowitz S, Iaquina PJ, Shamu T, Shukla S, et al. ETS factors reprogram the androgen receptor cistrome and prime prostate tumorigenesis in response to PTEN loss. *Nature medicine* 2013;19:1023–9
23. Lee AW. The role of atypical protein kinase C in CSF-1-dependent Erk activation and proliferation in myeloid progenitors and macrophages. *PLoS One* 2011;6:e25580 [PubMed: 22028782]
24. Zhu Y, Herndon JM, Sojka DK, Kim KW, Knolhoff BL, Zuo C, et al. Tissue-Resident Macrophages in Pancreatic Ductal Adenocarcinoma Originate from Embryonic Hematopoiesis and Promote Tumor Progression. *Immunity* 2017;47:323–38 e6 [PubMed: 28813661]
25. Stanley ER, Chitu V. CSF-1 receptor signaling in myeloid cells. *Cold Spring Harb Perspect Biol* 2014;6
26. Liu M, Cline J, Elkenawi A, Ruffell B, J. K. Analysis of Cholesterol and Androgens in Mouse Prostate Cells by LC-MS/MS: HESI versus APCI". 68th ASMS Conference on Mass Spectrometry 2020
27. Mills IG. Maintaining and reprogramming genomic androgen receptor activity in prostate cancer. *Nat Rev Cancer* 2014;14:187–98 [PubMed: 24561445]
28. Cancer Genome Atlas Research N. The Molecular Taxonomy of Primary Prostate Cancer. *Cell* 2015;163:1011–25 [PubMed: 26544944]
29. Westerterp M, Murphy AJ, Wang M, Pagler TA, Vengrenyuk Y, Kappus MS, et al. Deficiency of ATP-binding cassette transporters A1 and G1 in macrophages increases inflammation and accelerates atherosclerosis in mice. *Circ Res* 2013;112:1456–65 [PubMed: 23572498]
30. Ramji DP. Growth hormone-releasing peptides, CD36, and stimulation of cholesterol efflux: cyclooxygenase-2 is the link. *Cardiovascular Research* 2009;83:419–20 [PubMed: 19520704]
31. Chistiakov DA, Bobryshev YV, Orekhov AN. Macrophage-mediated cholesterol handling in atherosclerosis. *J Cell Mol Med* 2016;20:17–28 [PubMed: 26493158]
32. Goossens P, Rodriguez-Vita J, Etzerodt A, Masse M, Rastoin O, Gouirand V, et al. Membrane Cholesterol Efflux Drives Tumor-Associated Macrophage Reprogramming and Tumor Progression. *Cell Metab* 2019;29:1376–89 e4 [PubMed: 30930171]
33. He C, Hu X, Weston TA, Jung RS, Sandhu J, Huang S, et al. Macrophages release plasma membrane-derived particles rich in accessible cholesterol. *Proc Natl Acad Sci U S A* 2018;115:E8499–E508 [PubMed: 30127022]
34. Schiewer MJ, Goodwin JF, Han S, Brenner JC, Augello MA, Dean JL, et al. Dual roles of PARP-1 promote cancer growth and progression. *Cancer Discov* 2012;2:1134–49 [PubMed: 22993403]
35. Karlou M, Tzelepi V, Efstathiou E. Therapeutic targeting of the prostate cancer microenvironment. *Nat Rev Urol* 2010;7:494–509 [PubMed: 20818327]
36. Xu J, Escamilla J, Mok S, David J, Priceman S, West B, et al. CSF1R signaling blockade stanches tumor-infiltrating myeloid cells and improves the efficacy of radiotherapy in prostate cancer. *Cancer Res* 2013;73:2782–94 [PubMed: 23418320]
37. Escamilla J, Schokrpur S, Liu C, Priceman SJ, Moughon D, Jiang Z, et al. CSF1 receptor targeting in prostate cancer reverses macrophage-mediated resistance to androgen blockade therapy. *Cancer research* 2015;75:950–62 [PubMed: 25736687]
38. Ammirante M, Luo JL, Grivennikov S, Nedospasov S, Karin M. B-cell-derived lymphotoxin promotes castration-resistant prostate cancer. *Nature* 2010;464:302–5 [PubMed: 20220849]

39. Calcinotto A, Spataro C, Zagato E, Di Mitri D, Gil V, Crespo M, et al. IL-23 secreted by myeloid cells drives castration-resistant prostate cancer. *Nature* 2018;559:363–9 [PubMed: 29950727]
40. Di Mitri D, Toso A, Chen JJ, Sarti M, Pinton S, Jost TR, et al. Tumour-infiltrating Gr-1+ myeloid cells antagonize senescence in cancer. *Nature* 2014;515:134–7 [PubMed: 25156255]
41. Gannon PO, Poisson AO, Delvoye N, Lapointe R, Mes-Masson AM, Saad F. Characterization of the intra-prostatic immune cell infiltration in androgen-deprived prostate cancer patients. *J Immunol Methods* 2009;348:9–17 [PubMed: 19552894]
42. Miller WL, Auchus RJ. The molecular biology, biochemistry, and physiology of human steroidogenesis and its disorders. *Endocr Rev* 2011;32:81–151 [PubMed: 21051590]
43. Mahata B, Pramanik J, van der Weyden L, Polanski K, Kar G, Riedel A, et al. Tumors induce de novo steroid biosynthesis in T cells to evade immunity. *Nat Commun* 2020;11:3588 [PubMed: 32680985]
44. Yang Y, Bai Y, He Y, Zhao Y, Chen J, Ma L, et al. PTEN Loss Promotes Intratumoral Androgen Synthesis and Tumor Microenvironment Remodeling via Aberrant Activation of RUNX2 in Castration-Resistant Prostate Cancer. *Clinical cancer research : an official journal of the American Association for Cancer Research* 2018;24:834–46 [PubMed: 29167276]
45. Cai C, Chen S, Ng P, Bublely GJ, Nelson PS, Mostaghel EA, et al. Intratumoral de novo steroid synthesis activates androgen receptor in castration-resistant prostate cancer and is upregulated by treatment with CYP17A1 inhibitors. *Cancer research* 2011;71:6503–13 [PubMed: 21868758]
46. Leon CG, Locke JA, Adomat HH, Etinger SL, Twiddy AL, Neumann RD, et al. Alterations in cholesterol regulation contribute to the production of intratumoral androgens during progression to castration-resistant prostate cancer in a mouse xenograft model. *Prostate* 2010;70:390–400 [PubMed: 19866465]
47. Hales DB. Testicular macrophage modulation of Leydig cell steroidogenesis. *J Reprod Immunol* 2002;57:3–18 [PubMed: 12385830]
48. Watt MJ, Clark AK, Selth LA, Haynes VR, Lister N, Rebello R, et al. Suppressing fatty acid uptake has therapeutic effects in preclinical models of prostate cancer. *Science Translational Medicine* 2019;11:eaau5758 [PubMed: 30728288]
49. Traugher CA, Opoku E, Brubaker G, Major J, Lu H, Lorkowski SW, et al. Uptake of high-density lipoprotein by scavenger receptor class B type 1 is associated with prostate cancer proliferation and tumor progression in mice. *Journal of Biological Chemistry* 2020;295:8252–61
50. He C, Jiang H, Song W, Riezman H, Tontonoz P, Weston TA, et al. Cultured macrophages transfer surplus cholesterol into adjacent cells in the absence of serum or high-density lipoproteins. *Proceedings of the National Academy of Sciences* 2020;117:10476–83
51. Dupont M, Souriant S, Lugo-Villarino G, Maridonneau-Parini I, Vérollet C. Tunneling Nanotubes: Intimate Communication between Myeloid Cells. *Frontiers in Immunology* 2018;9
52. He C, Hu X, Weston TA, Jung RS, Sandhu J, Huang S, et al. Macrophages release plasma membrane-derived particles rich in accessible cholesterol. *Proceedings of the National Academy of Sciences* 2018;115:E8499–E508
53. Ong DS, Anzinger JJ, Leyva FJ, Rubin N, Addadi L, Kruth HS. Extracellular cholesterol-rich microdomains generated by human macrophages and their potential function in reverse cholesterol transport. *Journal of Lipid Research* 2010;51:2303–13 [PubMed: 20421591]
54. Tomlins SA, Rhodes DR, Perner S, Dhanasekaran SM, Mehra R, Sun XW, et al. Recurrent fusion of TMPRSS2 and ETS transcription factor genes in prostate cancer. *Science* 2005;310:644–8 [PubMed: 16254181]
55. Weischenfeldt J, Simon R, Feuerbach L, Schlangen K, Weichenhan D, Minner S, et al. Integrative genomic analyses reveal an androgen-driven somatic alteration landscape in early-onset prostate cancer. *Cancer Cell* 2013;23:159–70 [PubMed: 23410972]
56. Gerhauser C, Favero F, Risch T, Simon R, Feuerbach L, Assenov Y, et al. Molecular Evolution of Early-Onset Prostate Cancer Identifies Molecular Risk Markers and Clinical Trajectories. *Cancer Cell* 2018;34:996–1011 e8 [PubMed: 30537516]
57. Knuutila M, Mehmood A, Maki-Jouppila J, Ryberg H, Taimen P, Knaapila J, et al. Intratumoral androgen levels are linked to TMPRSS2-ERG fusion in prostate cancer. *Endocr Relat Cancer* 2018;25:807–19 [PubMed: 29773553]

58. Flaveny CA, Griffett K, El-Gendy Bel D, Kazantzis M, Sengupta M, Amelio AL, et al. Broad Anti-tumor Activity of a Small Molecule that Selectively Targets the Warburg Effect and Lipogenesis. *Cancer cell* 2015;28:42–56 [PubMed: 26120082]
59. Tavazoie MF, Pollack I, Tanquedo R, Ostendorf BN, Reis BS, Gonsalves FC, et al. LXR/ApoE Activation Restricts Innate Immune Suppression in Cancer. *Cell* 2018;172:825–40 e18 [PubMed: 29336888]
60. Wu G, Wang Q, Xu Y, Li J, Zhang H, Qi G, et al. Targeting the transcription factor receptor LXR to treat clear cell renal cell carcinoma: agonist or inverse agonist? *Cell Death Dis* 2019;10:416 [PubMed: 31138790]
61. Bousset L, Septier A, Bunay J, Voisin A, Guiton R, Damon-Soubeyrant C, et al. Absence of nuclear receptors LXRs impairs immune response to androgen deprivation and leads to prostate neoplasia. *PLOS Biology* 2020;18:e3000948 [PubMed: 33284790]

Significance

These results suggest that macrophage-targeted therapies can be combined with androgen deprivation therapy to treat prostate cancer patients by limiting cholesterol bioavailability and the production of intratumoral androgens.

Author Manuscript

Author Manuscript

Author Manuscript

Author Manuscript

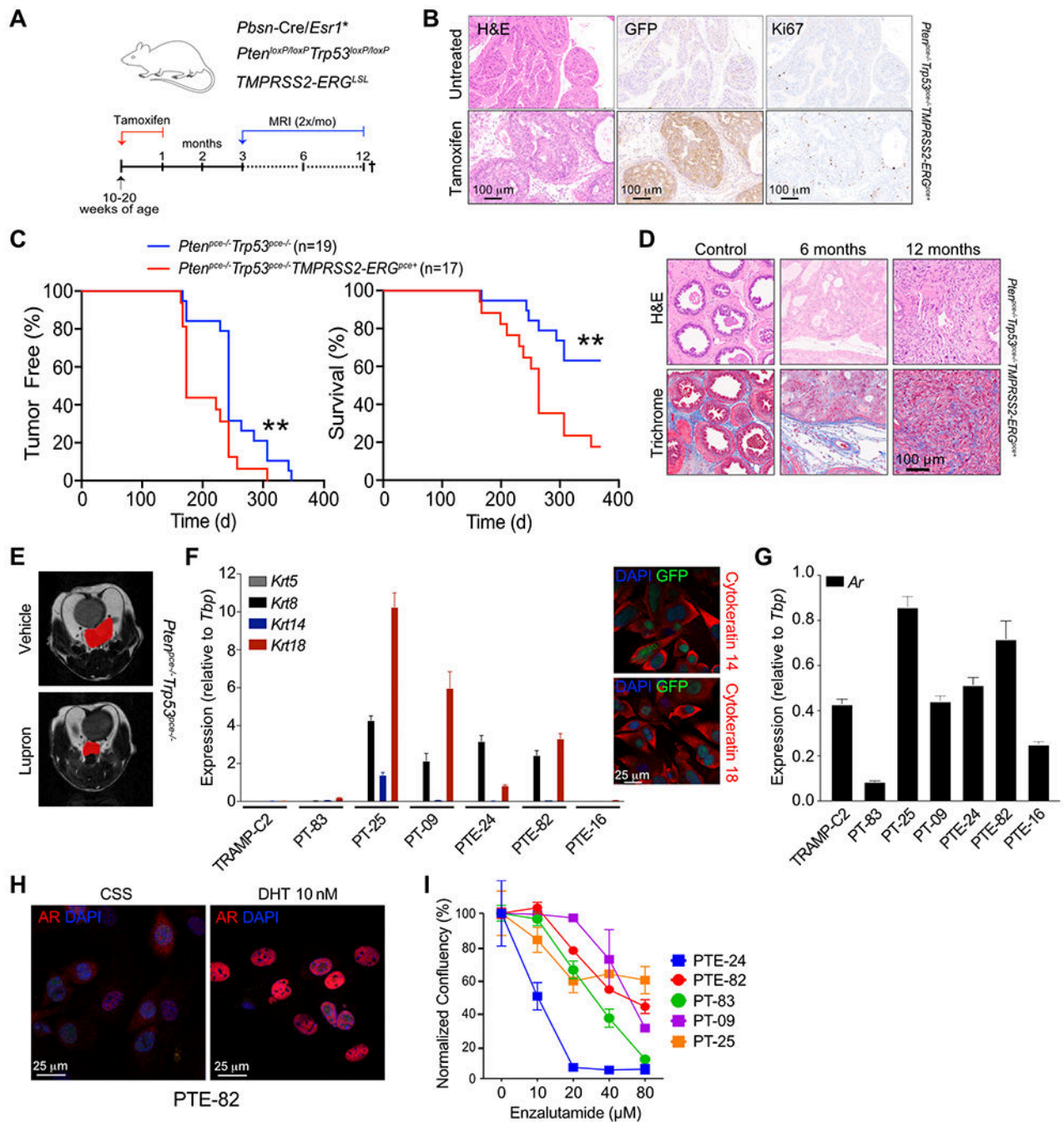


Figure 1. Development of syngeneic mouse models representing CRPC.

A) Mouse model scheme. B) Tamoxifen induced GFP and Ki67 expression in prostate glands of a *Pten^{pce}-/-/Trp53^{pce}-/-/TMPRSS2-ERG^{pce}+*</sup></sup></sup>* mouse after 2 month of tamoxifen administration, n=1. C) Detection of prostate tumors and overall survival in *Pten^{pce}-/-/Trp53^{pce}-/-</sup></sup>* and *Pten^{pce}-/-/Trp53^{pce}-/-/TMPRSS2-ERG^{pce}+*</sup></sup></sup>* mice. Days reflect time post tamoxifen administration. Tumor incidence and size were monitored by monthly MRI starting at 5-6 months. n=17-19 mice, pooled from two independent cohorts. Significance between the two groups was determined by log-rank. D) Hematoxylin and eosin (H&E)

and Masson's trichrome staining in *Pten*^{pce-/-}/*Trp53*^{pce-/-}/*TMPRSS2-ERG*^{pce+} mice from C. Control prostate glands were harvested from mice at 6 and 12 months of age. E) Representative T2-weighted image by MRI of tumor lesion-bearing *Pten*^{pce-/-}/*Trp53*^{pce-/-} mice treated with vehicle or 0.6 mg Lupron subcutaneously every 28 days for two cycles, starting 4 months after tamoxifen administration. n=3-5 mice per group, data from a one cohort of mice. F) Expression of *Krt5*, *Krt8*, *Krt14*, *Krt18* in the different cell lines generated from either *Pten*^{pce-/-}/*Trp53*^{pce-/-} (PT) or *Pten*^{pce-/-}/*Trp53*^{pce-/-}/*TMPRSS2-ERG*^{pce+} (PTE) mice at end-stage. n=6 from one cohort, with data shown as the mean \pm SEM. TRAMP-C2 cell line was used as a comparison. Representative confocal microscopy immunofluorescent images of the PTE-82 cell line stained for cytokeratin 14 and cytokeratin 18 are shown to the right. Similar results were obtained for the PT-09, PT-25, and PTE-24 lines. Images represent one of two independent experiments. G) Expression of *Ar* in the different cell lines. n=6 from one cohort, data shown as the mean \pm SEM. H) Confocal microscopy immunofluorescent images of the PTE-82 cell line either treated with 10 nM DHT or left untreated in charcoal stripped serum (CSS). Androgen receptor (red) and DAPI (blue). Images are representative of one of three independent experiments. I) Dose response curve of enzalutamide in 5 different prostate cancer cell lines. Phase contrast images were acquired at 8 hr intervals using Incucyte, with confluence per well calculated per cell line. n=3, data shown as the mean \pm SEM from one of at least three independent experiments.

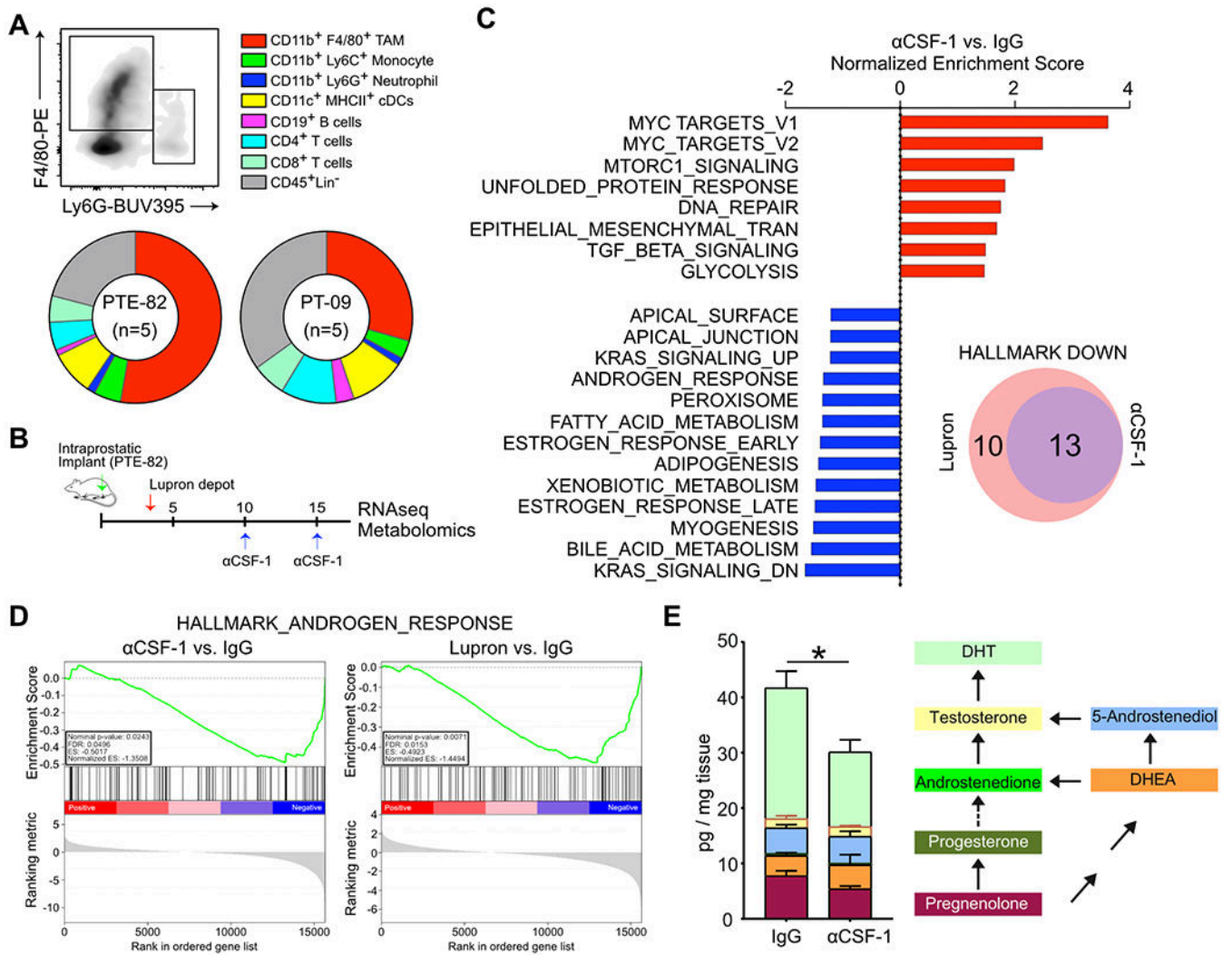


Figure 2. Macrophages are associated with cholesterol transport and steroid hallmarks.
 A) Immune infiltration in orthotopic models of prostate cancer, as determined by flow cytometry. n=5 mice per group, with results from one of three independent experiments shown as the mean. B) Treatment schematic for Lupron and α -CSF1. C) Gene set enrichment analysis (GSEA) following whole tumor RNA sequencing. The normalized enrichment score is shown comparing tumors from mice treated with α -CSF1 versus an IgG control. Data reflects 3 tumors per group from a single experiment. D) Enrichment plots of the Androgen Response Hallmark show for tumors from mice treated with α -CSF1 or Lupron, compared to the IgG control. E) LC-MS/MS quantification of pregnenolone, progesterone, androstenedione, DHEA, 5-androstenediol, testosterone and DHT in fresh tumor tissues. n=5-6 mice per group, from one of two independent experiments. Measurements were normalized by tissue weight. Significance determined by unpaired t test for DHT. *p<0.05.

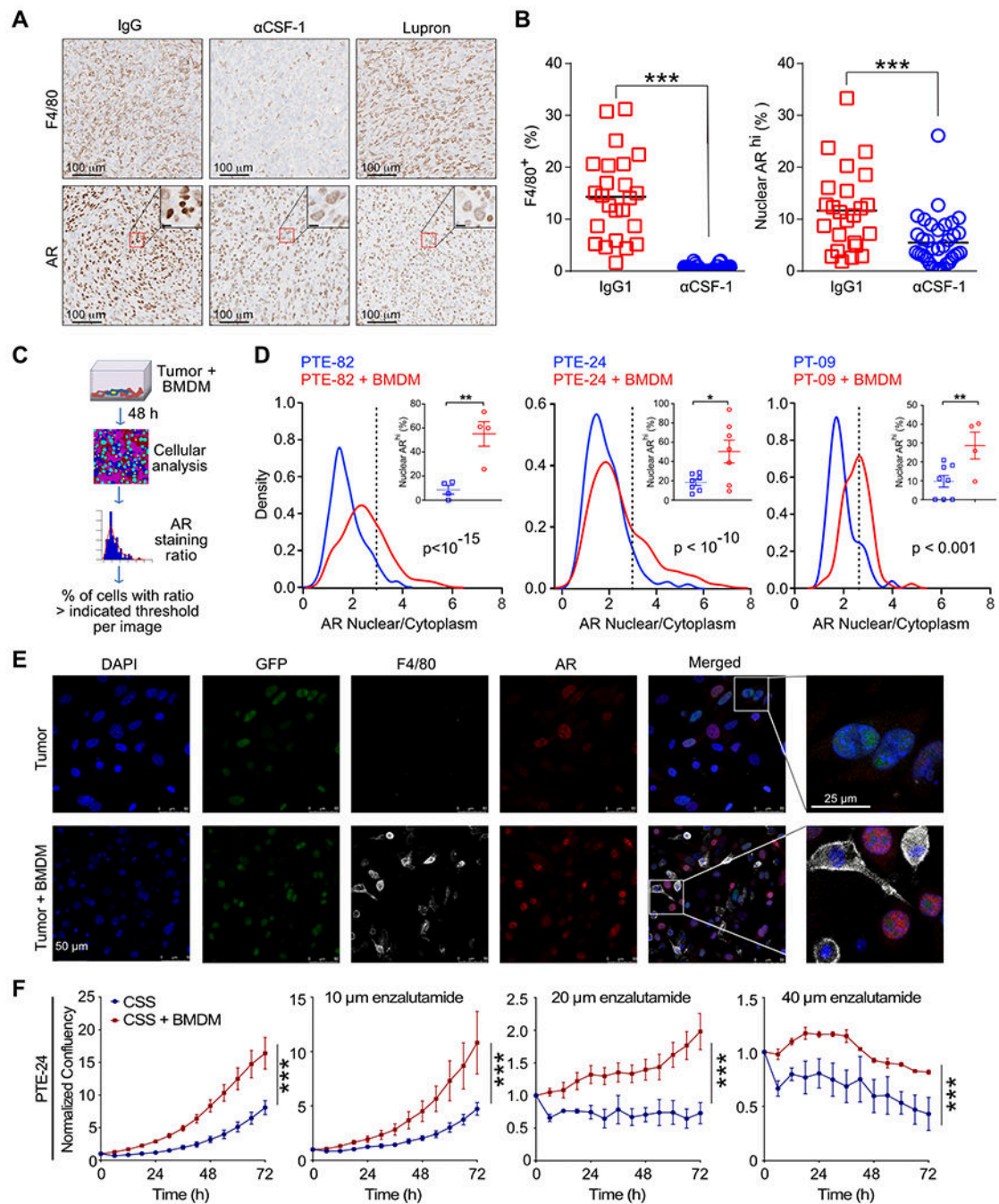


Figure 3. Macrophages directly regulate AR nuclear translocation.

A) Representative immunohistochemistry for tumor macrophages (F4/80) and AR within orthotopic prostate tumors from mice treated with IgG (control), α-CSF or Lupron. B) Quantification of the percent of F4/80⁺ cells and AR^{hi} nuclei in serial sections. n=5-6 mice per group from one of two independent experiments. 4-5 regions of interest (ROI) per each slide were selected in non-necrotic areas of the tumor. Significance determined by unpaired t test and shown as ***p<0.001. C) Experimental schematic for cancer cell and BMDM co-culture and quantification of nuclear AR by confocal microscopy. D) Kernel

density estimation of the AR nuclear to cytoplasmic ratio on a cell-by-cell basis following incubation of PTE-82, PTE-24 and PTE-09 cancer cell lines alone, or in co-culture with BMDMs under androgen-deprived conditions (i.e., charcoal-stripped serum, CSS) for 48 hrs. Percent of AR^{hi} cells was computed per individual images using the 3rd quartile of the nucleus/cytoplasm AR intensity ratio as a threshold (3rd quartile of PTE-82, PTE-24 or PTE-09 + BMDM = 3, 3, 2.4, respectively). n=3, data from one of at least three independent experiments. Significance determined by Mann-Whitney. E) Representative confocal microscopy images of the GFP⁺ PTE-24 cell line. AR (red), F4/80 (white) and DAPI (blue) fluorescence is shown. F) Impact of BMDMs on the proliferation of PTE-24 cells in the presence of serial concentrations of enzalutamide. Cell proliferation was monitored using live imaging with phase contrast images acquired every 6 hr. Data shown as the mean \pm SEM and reflects one of 2 independent experiments. Significance determined by two-way ANOVA.

Author Manuscript

Author Manuscript

Author Manuscript

Author Manuscript

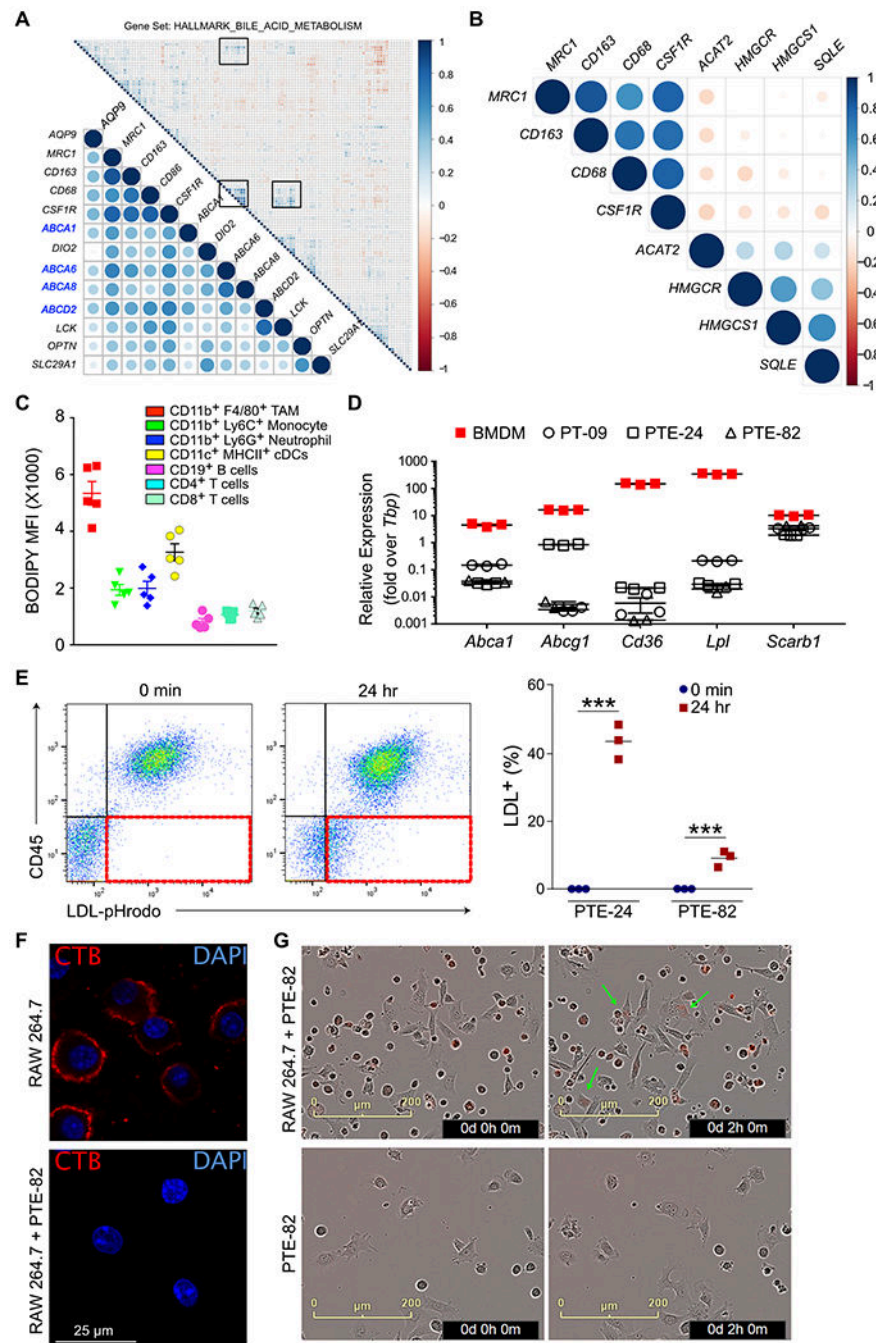


Figure 4. Macrophages transfer cholesterol to prostate cancer cells.

A) Intergene correlation analysis of genes associated with macrophage infiltration (*CD86*, *CSF1R*, *MRC1*, *CD163*) and bile acid metabolism from TCGA. B) Intergene correlation analysis of genes associated with macrophage infiltration and *de novo* cholesterol synthesis (*ACAT2*, *HMGCR*, *HMGCS1*, *SQLE*). Analysis was performed with the Corrplot package in R. Correlation coefficients are indicated by changes in circle color and size. C) Neutral lipid staining in immune cells within orthotopic PTE-82 tumors, as measured by BODIPY-493/503 staining in single cell suspensions. n=5 mice, data shown as the mean \pm

SEM from one of three independent experiments. D) Expression of cholesterol metabolism-related genes in prostate cancer cell lines and BMDMs. $n=3$, data from one of three independent experiments. E) RAW264.7 cells were loaded with human LDL covalently conjugated to pHrodo Red for 3 hrs, then co-cultured with prostate cancer cells for 24 hrs prior to flow cytometric analysis. Cells were cultured separately and then admixed just prior to data acquisition for the 0 min control. The acquisition of fluorescence by the CD45⁻ cancer cells is highlighted in the 3rd quadrant in red. Quantification of percent LDL-positive tumor cells is shown to the right. $n=3$ biological replicates from one of two independent experiments. Data are presented as mean \pm SEM. Student's *t* test was utilized for statistical analysis and is shown as *** $p < 0.001$. F) Immunofluorescence staining of cholesterol rich lipid rafts in the plasma membrane of RAW264.7 cells using Cholera toxin B (red). Cells were cultured alone or with PTE-82 cells in CSS for 48 hrs. Only nuclear GFP⁻ RAW264.7 cells are shown. $n=3$, data from one of two independent experiments. G) Live imaging of uptake of pHrodo Red-LDL (0.5 $\mu\text{g/ml}$) by PTE-82 tumor cells in the presence or absence of RAW264.7 cells. Arrows indicate tumor cells with red fluorescence. $n=3$, data reflects one of three independent experiments.

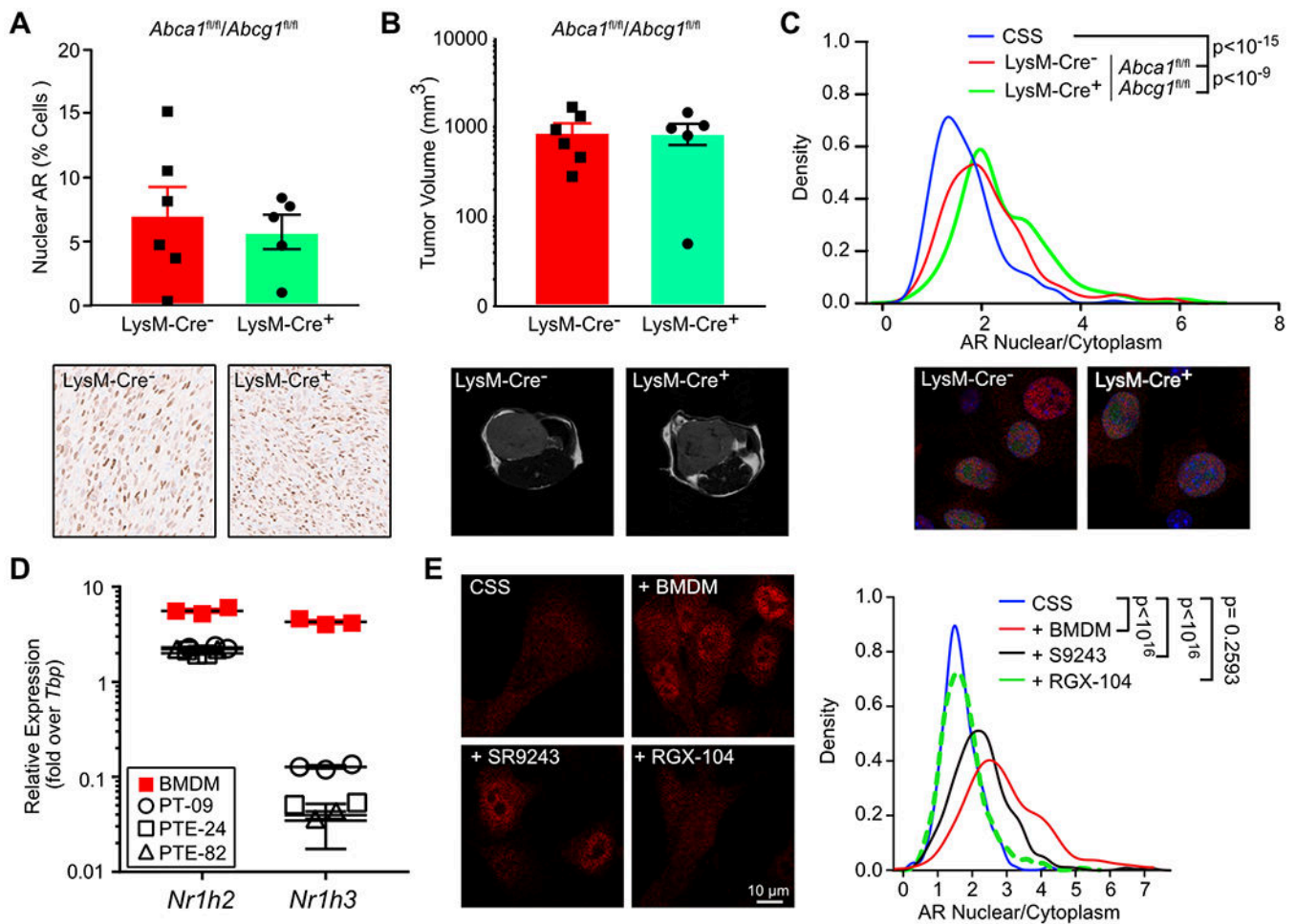


Figure 5. Perturbing cholesterol homeostasis inhibits macrophage-mediated AR translocation. A) PTE-82 prostate cancer cells were orthotopically injected into *LysM-Cre⁺/Abca1^{fl/fl}/Abcg1^{fl/fl}* or *LysM-Cre⁻/Abca1^{fl/fl}/Abcg1^{fl/fl}* and nuclear expression of AR was evaluated after 19 days by IHC. Representative images are shown below. n=5-6 mice per group from one of two independent experiments, data shown as the mean ± SEM. Significance was determined by unpaired *t* test assuming Gaussian distribution and with Welch's correction. B) Tumor volume in mice from A, as measured by MRI. Representative T2-weighted MRI images are shown. C) Nuclear to cytoplasmic AR ratio of GFP⁺ PTE-82 cells cultured in CSS, either alone or in the presence of BMDMs derived from *LysM-Cre⁺/Abca1^{fl/fl}/Abcg1^{fl/fl}* or *LysM-Cre⁻/Abca1^{fl/fl}/Abcg1^{fl/fl}* donors. 6-8 randomly selected images from two wells of the chamber slides were pooled for analysis. Data reflects one of three independent experiments. Significance was determined by Mann-Whitney. D) Expression of *Nr1h2* (LXRβ) and *Nr1h3* (LXRα) in prostate cancer cell lines and BMDMs. n=3, data shown as the mean ± SEM from one of two independent experiments. E) Nuclear to cytoplasmic AR ratio of GFP⁺ PTE-82 cells cultured in CSS or co-cultured with BMDMs. 5 μM SR9243 (LXRα/β inverse agonist) or 5 μM RGX-104 (LXRβ agonist) were added to co-cultures as indicated. 6-8 randomly selected images from two wells of the chamber slides

were pooled for analysis. Data reflects one of three independent experiments. Significance determined by Mann-Whitney.

Author Manuscript

Author Manuscript

Author Manuscript

Author Manuscript

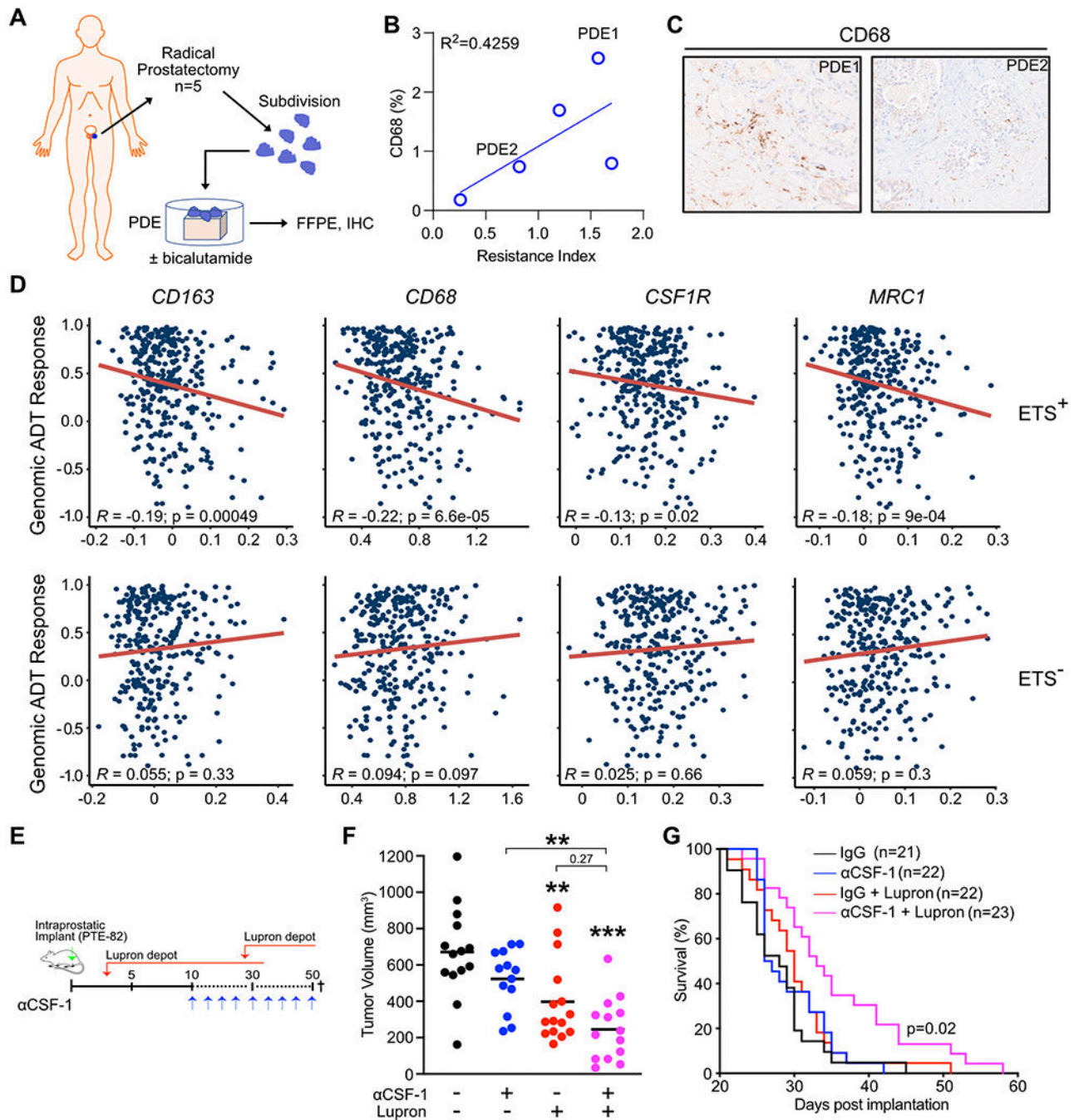


Figure 6. Macrophage depletion sensitizes CRPC to Lupron.

A) Diagram demonstrating set up of PDEs and treatment with bicalutamide (BIC). B,C) 4 μM sections from PDEs were stained with CD68. Response to bicalutamide was determined by the ratio between the number of nuclei/mm² in sections obtained from bicalutamide PDEs and number of nuclei/mm² in sections prepared from control treated PDEs. D) Expression of macrophage-associated genes was correlated with ADT response score, with stratification by ETS status. F) PTE-82 tumor cells were implanted orthotopically into prostates of C57 mice, which were then treated with Lupron depot and/or $\alpha CSF-1$ as

indicated. Tumor volumes for individual mice are shown for day 21. n=13-15 mice per group, data pooled from two independent experiments. Significance was determined by one-way ANOVA and is show compared to the IgG control group, unless otherwise indicated. G) Tumor volume in treatment groups as measured by MRI. H) Survival as determine by tumor volume or organ obstruction. n=21-23 mice, data pooled from three experiments. Significance was determined via log-rank.

Author Manuscript

Author Manuscript

Author Manuscript

Author Manuscript